STABILIZED FIBER OPTIC SENSOR FOR ULTRASOUND DETECTION

J. Dorighi
S. Krishnaswamy
J.D. Achenbach
Center For Quality Engineering and Failure Prevention
Northwestern University
Evanston, IL 60208

INTRODUCTION

Fiber optic sensors are emerging as important new tools in the field of nondestructive evaluation (NDE). They offer a number of advantages over sensing elements traditionally used in NDE applications such as resistive foil strain gauges and piezoelectric transducers. The advantages of fiber optic sensors over traditional NDE sensors include: ease of embedding in composite materials, good mechanical interaction between the embedded sensor and the host structure, insensitivity to electrical interference, and fine spatial resolution [1]. Additionally, fiber optic sensors can be configured to detect a variety of fields from large slowly varying thermal and mechanical strains, to ultrasound and acoustic emission. They have shown potential in a variety of material systems such as graphite/epoxy composites [2], titanium matrix composites [3], aluminum [4], and concrete [5]. They have also been embedded in a number of practical structures including airplanes [6][7], buildings [8][9], and dams [10].

We have chosen the intrinsic fiber optic Fabry-Perot (FOFP) as our fiber sensor. This type of sensor is a truly localized fiber interferometer which requires the installation of only one fiber length per sensor. The FOFP has been successfully configured for the detection of both strain and temperature [11-16]. However, its potential as a useful tool in NDE ultrasound applications remains largely untapped. Several authors have demonstrated the capability of FOFPs for ultrasound detection using unstabilized sensors.[17][18] However, stabilization is a key issue which must be addressed before practical applications of this sensor can be realized. In this work we will discuss an active homodyne technique which stabilizes the FOFP by tuning the laser frequency. Resulting improvements in sensitivity when detecting ultrasound will be demonstrated.

PRINCIPLES OF OPERATION

The fiber optic Fabry-Perot consists of a partially mirrored fiber end face spliced to a small fiber length that has been completely mirrored at the other end, as shown by the schematic in Figure 1. This sensor detects phase shifts of light in the sensing fiber produced by changes in length and refractive index of the sensor. Light propagates through the reference fiber until it reaches the partial mirror where a portion is transmitted into the sensing region. This light undergoes a phase shift which is manifested as a change in reflected intensity upon interfering with light in the reference fiber at the partial mirror.

Review of Progress in Quantitative Nondestructive Evaluation, Vol. 14
Edited by D.O. Thompson and D.E. Chimenti, Plenum Press, New York, 1995

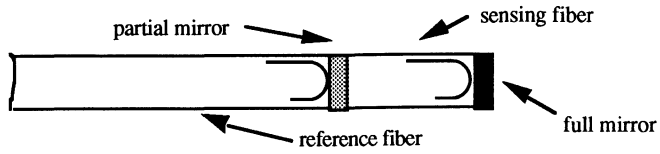

Figure 1: Schematic of FOFP.

An expression for the static phase shift of light in the sensing region is given by

$$\varphi = \frac{4\pi v \ell n}{c} \tag{1}$$

where: ℓ is the gauge length of the sensor, v is the frequency of the light, n is the refractive index of the fiber, and c is the speed of light in a vacuum . For a FOFP with low reflectivity mirrors which is termed low finesse, the reflected intensity as a function of phase shift is expressed as

$$P_r = 2RP_i(1-\cos\varphi) \tag{2}$$

where: P_r is the intensity of reflected light, P_i is the intensity of incident light, R is the reflectivity of the mirrors, and φ is the static phase shift of the light in the sensing region. The reflected intensity as a function of phase shift is plotted in Figure 2. We can see that for large phase shifts the reflected intensity oscillates through many peaks. However, for displacements much less than the wavelength of laser light, only local oscillations about a point will occur. Typical displacements associated with ultrasound are small, 1 to 50 nm [19], compared to the wavelength of light we are using, 780 nm. Consequently, we expect local oscillations about a point to result. It is desirable to make measurements along the linear region of the response curve, the region between the peaks and valleys. This is known as quadrature and gives the largest change in reflected intensity for a given phase shift of light.

The intrinsic FOFP sensor must be actively maintained at quadrature due to drift of the sensor response. Drift in the fiber interferometer results from laser frequency fluctuations along with mechanical and temperature induced strains. An active homodyne technique has been demonstrated by Jackson et al [20] to compensate for drift in a Mach-Zender fiber interferometer. This technique used a piezoelectric fiber stretcher to control the reference fiber length such that quadrature was maintained. Liu et al [21] have applied this technique to stabilize an embedded Michelson fiber interferometer used to detect ultrasound. We are unable to use a piezoelectric element to stabilize the FOFP because the sensor gauge length is embedded, prohibiting access to a fiber stretcher. Consequently, we have employed an active homodyne technique which modulates the laser frequency in order to maintain quadrature. This stabilization method has previously been demonstrated by Dandridge and Tveten [22] who stabilized a Mach-Zender fiber interferometer.

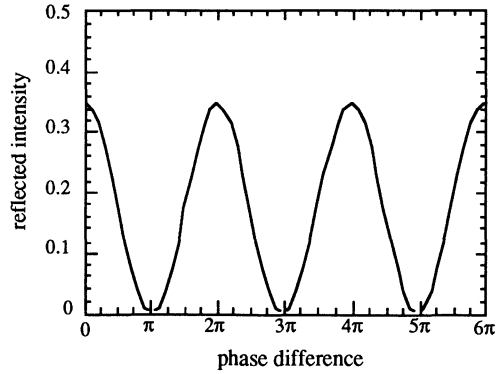

Figure 2: Normalized reflected intensity vs. phase shift.

EXPERIMENTAL APPARATUS

We have chosen active homodyne stabilization to maintain quadrature in an embedded Fabry-Perot sensor by tuning the laser frequency. The laser used to achieve this is an external cavity diode laser. This laser offers several advantages over traditional laser diodes including: narrower line width, greater frequency stability, and no mode hops over the tuning range. All of these advantages increase the sensitivity of the embedded fiber sensor.

Light from an external cavity tunable diode laser (New Focus at 780nm) passes through an optical isolator (Optics for Research Model IO-2-780) and is coupled into an ordinary single mode fiber (York fiber at 633 nm) using a coupling stage (Newport Model F-915). The fiber sensor (10 mm gauge length) was purchased from FiberMetrics and embedded in an epoxy block (1.5" x 1.5" x 3.0"). Light reflected back from the gauge length was directed toward a photodetector (Thor Labs Model PDA-150) using a beamsplitter. A schematic of the experimental setup is displayed in Figure 3. Recalling equation (2) we expect the back reflected intensity to be a sinusoid of constant amplitude if the frequency of the laser is shifted. However, using the experimental arrangement shown in Figure 3 and measuring the back reflected intensity as the laser frequency is shifted we find the sensor response consists of a high frequency sinusoid superimposed on one of lower frequency as shown in Figure 4. This indicates that actually two sensing cavities are present: a primary cavity formed by the partial and full mirrors of the local FOFP and a secondary cavity which consists of the mirror on the embedded end and the reflectance from the air/glass interface at the input end. In order for the embedded FOFP to be localized, the reflections from the input end must be eliminated through the use of an AR coating. However, to demonstrate the effectiveness of the stabilization scheme we have stabilized a nonlocal FOFP formed from a full mirror deposited on the embedded fiber endface and the air/glass interface at the input end.

STABILIZATION OF NONLOCAL FIBER OPTIC FABRY-PEROT

In order to implement active homodyne stabilization we must distinguish thermal and mechanical induced drifts from the ultrasonic signals of interest. This is done by noting that incident ultrasound frequencies are in a bandwidth from 100 kHz to 10 MHz, which is much higher than the variation due to mechanical strain and temperature, which is typically less than 500 Hz. We will track low frequency intensity variations and use a feedback loop with an integral controller to change the laser frequency and bring the interferometer back into quadrature.

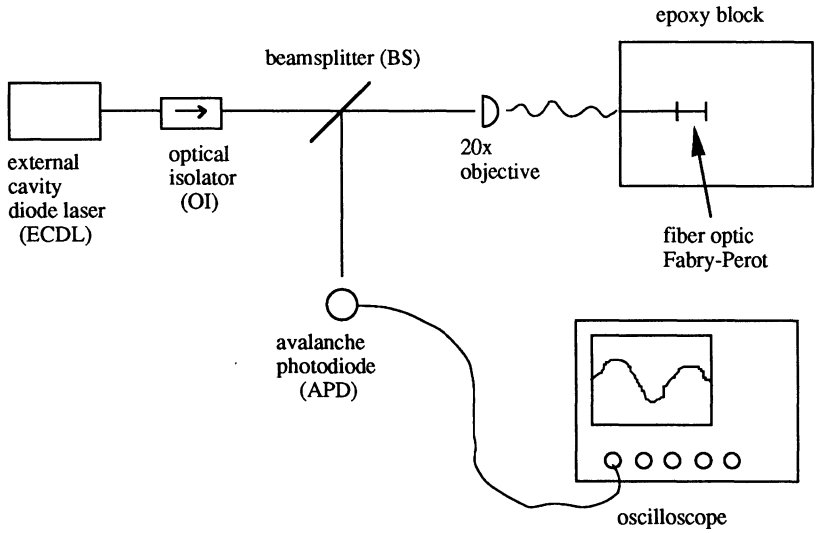

Figure 3: Schematic of experiment with local FOFP.

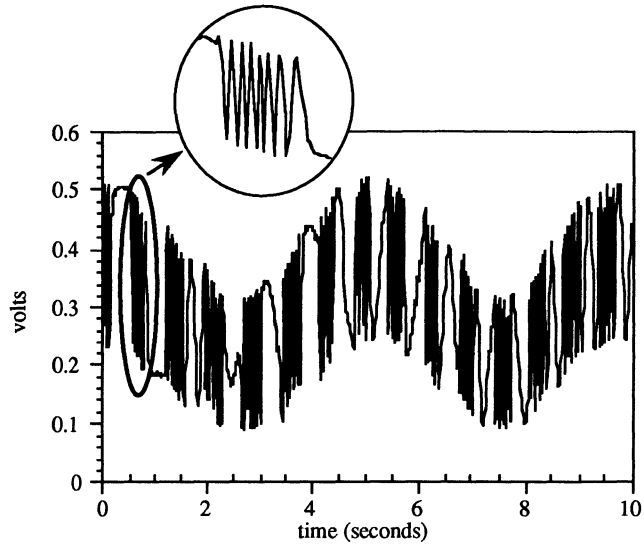

Figure 4: Reflected intensity from double cavity as frequency is shifted.

A schematic of the experimental arrangement used to stabilize a nonlocal FOFP is displayed in Figure 5. Light from the external cavity diode laser passes through an optical isolator and is coupled into the nonlocal FOFP with a coupling stage. The nonlocal FOFP is constructed from ordinary single mode fiber (3M at 633nm) and the sensing region is 1 meter long formed between a full mirror deposited on the embedded end and reflection from the air/glass interface at the input end. Light reflected back from the sensing region is directed toward two photodetectors using beamsplitters. The first photodetector, APD #1 (Hamamatsu Model C5331-02), is used to detect high frequency intensity variations caused by the incident ultrasound and its signal is input directly to a digital oscilloscope (Tektronix Model TDS-420). The second photodetector, APD #2 (Thor Labs Model PDA-150), is used in conjunction with the feedback loop to stabilize for low frequency intensity variations associated with drift of the sensor.

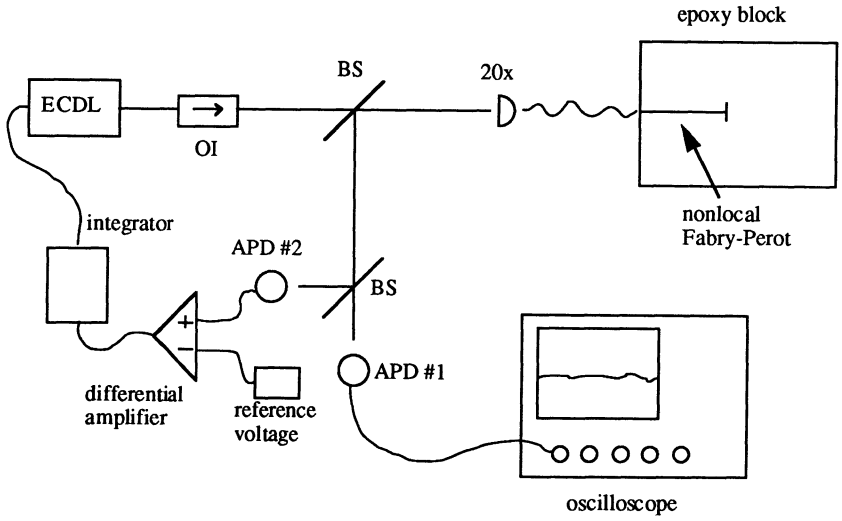

Figure 5: Schematic of experiment for stabilization of nonlocal FOFP.

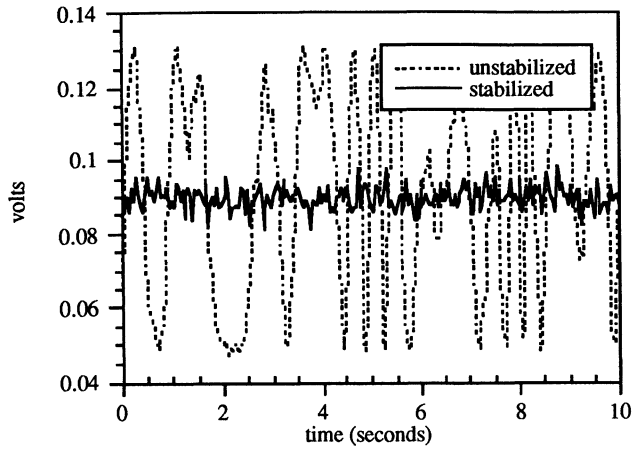

Figure 6: Reflected intensity from stabilized and unstabilized nonlocal FOFP.

The sensor was stabilized by comparing the voltage output from APD #2 to a reference voltage, representing the quadrature point of the interferometer, using a differential amplifier. The error signal produced by the differential amplifier indicates how much the embedded fiber interferometer is out of quadrature. This error signal is input to an op-amp integrator, determining the frequency response of the stabilization system, and finally connected to the laser which completes the stabilization loop. As the embedded interferometer drifts out of quadrature an error voltage is sent to the laser which shifts the light frequency by an appropriate amount bringing the system back into quadrature. In order to demonstrate the active homodyne stabilization applied to our sensor, the output from APD#2 was monitored with the nonlocal FOFP, both stabilized and unstabilized. Both of these cases are displayed in Figure 6, where time is displayed on the horizontal axis and volts are on the vertical axis. We see for the unstabilized configuration the reflected intensity drifts through many peaks on the response curve. However, when the sensor is stabilized the quadrature point is maintained.

The results displayed in Figure 6 indicate that drifts induced by a non hostile laboratory environment can be compensated for using the described active homodyne stabilization. In order to test the robustness of this stabilization technique, we used a heat gun to simulate a hostile environment which induced substantially more drift in our system. The approach used was to apply bursts from a heat gun at approximately 2 second intervals onto the exposed portion of the nonlocal FOFP. While this noise source is not strictly repeatable, it gives us a rough measure of the drifts our system can compensate for. Again we monitored the output from APD#2 with the heat gun applied when the system was stabilized and unstabilized. The drift of the nonlocal FOFP with the heat gun applied is displayed in Figure 7, where time is on the horizontal axis and volts are on the vertical axis. If we compare this to the unstabilized plot in Figure 6 we note that substantially more drift is induced when the heat gun is applied. When the nonlocal FOFP was stabilized with the heat gun applied, as shown in Figure 8, we see that peaks in the reflected intensity occur. These peaks result when the laser tuning range has been reached and the stabilization system can no longer compensate for drifts induced by the heat gun. The finite laser tuning range, 60 GHz, is the limiting factor of this technique but could be compensated for by incorporating a reset switch on the integrator. Such a switch would automatically reset when the tuning range of the laser is exceeded.

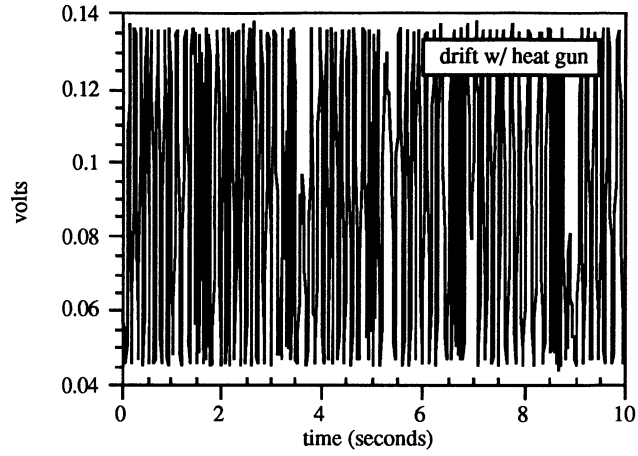

Figure 7: Reflected intensity from unstabilized nonlocal FOFP with heat gun induced drift.

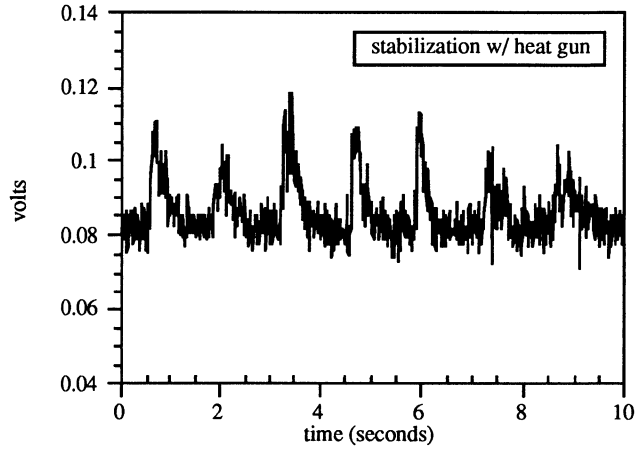

Figure 8: Reflected intensity from stabilized nonlocal FOFP with heat gun induced drift.

ULTRASOUND DETECTION

The nonlocal FOFP sensor displayed in Figure 5 has been used to detect ultrasound. Ultrasound was generated using a 5 MHz piezoelectric transducer (Panametrics) in conjunction with a function generator (Wavetek Model 395) and power amplifier (ENI Model 325LA). The transducer was placed on the epoxy block such that the face of the transducer was parallel to the direction of the embedded fiber. Three different amplitude tonebursts were input to the transducer generating elastic waves in the epoxy, which were detected using the nonlocal FOFP. The reflected intensity variations produced by the fiber sensor were sensed using APD #1 with the embedded FOFP stabilized and unstabilized. The results displayed in Figures 9a)-9f) are averaged 1000 times, where the horizontal axes are time and the vertical axes are volts. The signals detected by the stabilized and unstabilized nonlocal FOFP for the smallest amplitude toneburst are shown in Figures 9a) and 9b). We see that no ultrasound is detected unless the FOFP is stabilized. As the amplitude of the incident ultrasound is increased, the signals detected with the system stabilized are shown in Figures 9c) and 9e) and with the system unstabilized in Figures 9d) and 9f). Again we see that even at larger input amplitudes no ultrasound is detected unless the embedded sensor is stabilized .

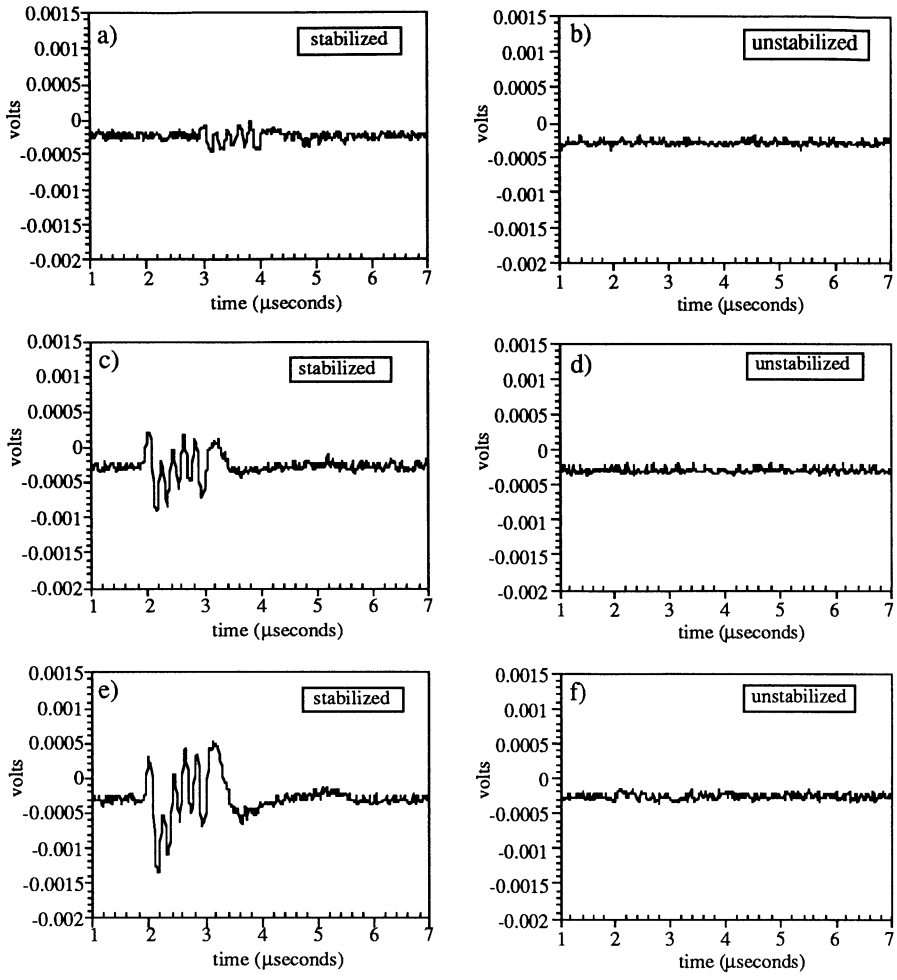

Figure 9: 5MHz toneburst detected with nonlocal FOFP stabilized and unstabilized.

CONCLUSIONS

We have demonstrated that a nonlocal FOFP can be maintained at quadrature using active homodyne stabilization which modulates the laser frequency. The limiting factor in this stabilization scheme is the laser tuning range of 60 GHz. The embedded stabilized sensor was used to detect 5 MHz tonebursts generated by a piezoelectric transducer. Three different input amplitudes were detected only when the embedded fiber sensor was stabilized.

Improvements which must be made to the present system include: application of an AR coating on the input fiber endface to eliminate the nonlocal secondary cavity, and incorporation of a reset switch on the integrator to compensate for limitations of the laser tuning range.

ACKNOWLEDGMENTS

This work is supported by the Air Force Office of Sponsored Research under Award#: F4960-92-J-0342AFOSR.

REFERENCES

1. R.M. Measures, *Fiber Optics Smart Structures Program at UTIAS*, SPIE Vol. 1170, (1989), p.92
2. C.E. Lee et al, *Optical Fiber Fabry-Perot Embedded Sensor*, Optics Letters, Vol. 14, No. 21, (1989), p.1225
3. S. Baldini et al, *Embedding Fiber Optic Sensors in Titanium Matrix Composites*, SPIE Vol. 1370, (1980), p.162
4. C.E. Lee et al, *Meihod for Embedding Optical Fibers and Optical Fiber Sensors in Metal Parts and Structures*, SPIE Vol. 1588, (1991), p.110
5. K.A. Mendez et al, *Overview of Optical Fiber Sensors Embedded in Concrete*, SPIE Vol. 1798, (1992), p.205
6. K.A. Murphy et al, *Fabry-Perot Fiber Optic Sensors in Full-Scale Fatigue testing on an F-15 Aircraft*, SPIE Vol. 1588, (1991), p.134
7. M. LeBlanc et al, *Development of a Fiber Optic Damage Detection System for an Aircraft Leading Edge*, SPIE Vol. 1170, (1989), p.196
8. A. Mendez et al, *Applications of Embedded Optical Fiber Sensors in Reinforced Concrete Buildings and Structures*, SPIE Vol. 1170, (1989), p.60
9. T.P. Ambrose et al, *Lessons Learned Embedding Fiber Sensors into Large Civil Structures*, SPIE Vol. 1798, (1992), p.194
10. P.L. Fuhr et al, *Multiplexed Fiber Optic Pressure and Vibration Sensors for Hydroelectric Dam Monitoring*, SPIE Vol 1798, (1992), p.247
11. C.E. Lee et al, *Interferometric Optical Fiber Sensors using Internal Mirrors*, Electronics Letters, Vol. 24, No. 4, (1988), p.193
12. C.E. Lee et al, *Performance of a Fiber-Optic Temperature Sensor from -200 to 1050 C*, Optics Letters, Vol. 13, No. 11, p.1038
13. C.E. Lee et al, *Optical Fiber Fabry-Perot Embedded Sensor*, Optics Letters, Vol. 14, No. 21, (1989), p.1225
14. T. Valis et al, *Fiber Optic Fabry-Perot Strain Gauge*, IEEE Photonics Technology Letters, Vol. 2, No. 3, (1990), p.27
15. K.A. Murphy et al, *Quadrature Phase-Shifted Extrinsic Fabry-Perot Optical Fiber Sensors*, Optics Letters, Vol. 16, No. 4, (1991), p.273
16. G.P. Carmen et al, *Implementation and Evaluation of an Embedded Extrinsic Fabry-Perot Fiber Optic Strain Rosette Sensor*, SPIE Vol. 1798, (1992), p.237
17. J.J. Alcoz et al, *Embedded Fiber-Optic Fabry-Perot Ultrasound Sensor*, IEEE Trans. Ultrasonics, Ferroelectrics, and Frequency Control, Vol. 37, No. 4, (1990), p.302
18. C.E. Lee et al, *Metal Embedded Fiber Optic Fabry-Perot Sensors*, Optics Letters, Vol. 16, No. 24, (1991), p.1990
19. J.W. Wagner, *Optical Detection of Ultrasound*, Physical Acoustics, Academic Press, Vol. XIX, (1990), p.208
20. D.A. Jackson et al, *Elimination of Drift in a Single-Mode Optical Fiber Interferometer using a Piezoelectrically Stretched Coiled Fiber*, Applied Optics, Vol. 19, No. 17, (1980), p.2926
21. K. Liu et al, *Detection of High-Frequency Elastic Waves with Embedded Ordinary Single-Mode Fibers*, SPIE Vol. 1584, (1991), P.226
22. A. Dandridge et al, *Phase Compensation in Interferometric Fiber-Optic Sensors*, Optics Letters, Vol. 7, No. 6, (1982), p.279